Multipoint Monin–Obukhov Similarity and Its Application to Turbulence Spectra in the Convective Atmospheric Surface Layer

CHENNING TONG AND KHUONG X. NGUYEN

Department of Mechanical Engineering, Clemson University, Clemson, South Carolina

(Manuscript received 14 May 2015, in final form 28 July 2015)

ABSTRACT

A generalized Monin–Obukhov similarity hypothesis for the atmospheric surface layer is proposed. It employs the Monin–Obukhov length as a length scale in both the horizontal and vertical directions, in contrast to the original Monin–Obukhov similarity. Therefore, the horizontal turbulence scales, which are contained in multipoint statistics, must be explicitly included. The similarity hypothesis is formulated for the joint probability density function (JPDF) of multipoint velocity and temperature differences and is termed the multipoint Monin–Obukhov similarity (MMO). In MMO, the nondimensional JPDF in the surface layer depends on the separation vectors and the heights from the ground, both nondimensionalized by the Monin–Obukhov length. A key aspect of MMO is that at heights much smaller than the absolute value of the Monin–Obukhov length, both shear and buoyancy can be important. As an application, MMO is used to predict the two-dimensional horizontal turbulence spectra in the convective surface layer. It predicts a two-layer structure with three scaling ranges. Comparisons of the predicted spectra with those obtained using high-resolution large-eddy simulations show general agreement, supporting MMO. Within MMO, full similarity is only achieved for multipoint statistics, while similarity properties (or a lack thereof) for one-point statistics (the original Monin–Obukhov similarity) can be derived from those of multipoint statistics. MMO provides a new framework for analyzing the turbulence statistics and for understanding the dynamics in the atmospheric surface layer.

1. Introduction

The Monin–Obukhov similarity hypothesis (Monin and Obukhov 1954; referred to as the M–O similarity) is the theoretical foundation for understanding the surface layer of the atmospheric boundary layer (ABL). According to the M–O similarity theory, for a distance from the ground z much smaller than the boundary layer depth z_i, the nondimensional turbulence statistics are determined by z/L, where L is the Monin–Obukhov length, the absolute value of which represents the height at which the buoyancy and shear production rates of turbulent kinetic energy are of the same order. Subsequent measurements have shown that many one-point statistics (e.g., those containing the vertical velocity) in the surface layer indeed follow the M–O similarity (Wyngaard and Coté 1971; Wyngaard et al. 1971). The horizontal velocity variances, however, are not M–O similar in the convective surface layer (e.g., Lumley and Panofsky 1964). They instead follow the mixed-layer scaling (Willis and Deardorff 1974).

In an effort to explain the observed deviation from the M–O similarity, Zilitinkevich (1971) proposed new formulations for the horizontal velocity statistics using directional dimensional analysis. Using the same approach, Betchov and Yaglom (1971) proposed a three-layer model for the structure of the convective atmospheric surface layer. The validity of directional dimensional analysis, however, depends on the horizontal and vertical velocities being decoupled, which is generally not the case in the convective surface layer.

Although similarity for two-point statistics was not included in the original formulation by Monin and Obukhov (1954), Kaimal et al. (1972) and Kaimal (1978) observed that while inertial-range spectra follow the M–O similarity, the large-scale spectra of the horizontal velocity components do not. Bradshaw (1978) attributed this to the contributions of the large-scale inactive

Corresponding author address: Prof. Chenning Tong, Department of Mechanical Engineering, 248 Fluor Daniel Building, Clemson University, Clemson, SC 29634.
E-mail: ctong@ces.clemson.edu

DOI: 10.1175/JAS-D-15-0134.1

motions. A general form of the velocity spectra was given by Yaglom (1994),

$$u_*^2 k^{-1} \phi_\alpha(kz, z/L), \tag{1}$$

where k is the horizontal wavenumber and ϕ_α is a nondimensional spectral function for $\alpha = u, v,$ and w. The Monin–Obukhov length is defined as $L = -u_*^3/(\kappa\beta Q)$, where u_*, κ, $\beta = g/T$, and Q are the friction velocity, the von Kármán constant, the buoyancy parameter, and the surface temperature flux, respectively. Kader (1988) and Kader and Yaglom (1991) predicted the horizontal velocity and temperature spectra in the three proposed sublayers of the convective surface layer ($-z/L \gg 1$, $-z/L \approx 1$, and $-z/L \ll 1$). Their prediction of the spectra in the dynamic layer ($-z/L \ll 1$) is identical to that of a neutral boundary layer, effectively assuming that buoyancy effects are not important in this layer. Thus, in this formulation of the M–O similarity, the dependence on the stability was assumed (explicitly or implicitly) to be only through z/L; that is, a spectrum has different scaling exponents for different z/L but not for different wavenumber ranges (e.g., $-kL \ll 1$ and $-kL \gg 1$). [Note that the parameter kz is used in Eq. (1) instead of kL. Panofsky and Dutton (1984) use kL, but only for the vertical velocity spectrum.] This is equivalent to assuming that the buoyancy effects depend only on the height from the ground, not on the horizontal length scale. We believe that this assumption prevents proper scaling of the horizontal velocity spectra.

The issues discussed above are due to two (implicit) assumptions that the M–O similarity makes. First, it assumes that the energy-containing eddies scale with z; therefore (nondimensional) one-point statistics are expected to depend on z/L only. This is in fact not the case in the convective surface layer. Second, in previous applications to the large-scale spectra (two-point statistics), $|L|$ was assumed to be a vertical length scale only, while z was used to nondimensionalize the horizontal wavenumber. Thus, as we will point out in section 2, the similarity formulation does not contain the correct nondimensional horizontal wavenumber.

In the present work we propose a generalized M–O similarity without these assumptions. It is based on both the vertical length scale z and the horizontal length scale (e.g., the horizontal wavenumber k), both nondimensionalized by the Monin–Obukhov length. To include the horizontal scales, it must be formulated for multipoint statistics; therefore, we term the generalized similarity the multipoint M–O similarity (referred to as MMO). We introduce the MMO framework in section 2. As an application of MMO, in section 3 we predict the velocity and temperature spectra in the convective atmospheric surface layer. These predictions are tested using large-eddy simulation (LES) data in section 4. The relationship between MMO and the (original) M–O similarity is discussed in section 5, followed by the conclusions.

2. Multipoint M–O similarity

The key to establishing MMO is the recognition that the Monin–Obukhov length is not only an important length scale in the vertical direction but also in the horizontal direction. The formulation is partly motivated by our recent studies of the convective surface-layer dynamics (Nguyen et al. 2013; Nguyen and Tong 2015), which show that the pressure–strain-rate correlation transfers turbulent kinetic energy from the smaller vertical velocity component to the larger horizontal ones. Furthermore, the cospectrum of the pressure and the strain rate shows that the vertical and horizontal velocity components are coupled at large scales (low horizontal wavenumbers) (Nguyen et al. 2014). Meanwhile, the large downward pressure transport of vertical velocity variance previously observed (Wyngaard and Coté 1971) indicates that the vertical velocity near the surface is coupled to that at greater heights ($z > -L$). The pressure–strain-rate correlation and the nonlocal pressure transport suggest that the (large scale) horizontal velocity fluctuations at $-z/L \ll 1$ are coupled to the motions at $-z/L \gg 1$. Thus, a horizontal length scale (e.g., $1/k$) is also representative of the vertical length scale, since when $zk \ll 1$, z is no longer a measure of the vertical length scale ($1/k$). Therefore, buoyancy effects, which are dominant at $-z/L \gg 1$, are also important for large horizontal length scales at heights $-z/L \ll 1$. The horizontal turbulence length scale is therefore also an important parameter for buoyancy effects.

This coupling can also be seen from the point of view of eddy structure in the convective surface layer. Since the large eddies in the surface layer are assumed to be "attached" to the surface (Townsend 1961, 1976), an eddy with a horizontal length scale $1/k \gg -L$ has a vertical length scale $\sim 1/k \gg -L$. Its vertical velocity gains energy from buoyancy production, which is transferred to the horizontal components by the eddy motions, thereby generating horizontal velocity fluctuations of scale $1/k$ even for heights $z \ll -L$. This implies that, even at a height $z \ll -L$, buoyancy effects can be important for the dynamics of the horizontal velocity fluctuations at large scales. The ratio of the horizontal scale of the eddies to L is therefore the most important parameter for the dynamics in this region, for both the vertical velocity and horizontal velocity statistics. Note that when a horizontal scale is explicitly used, kL rather

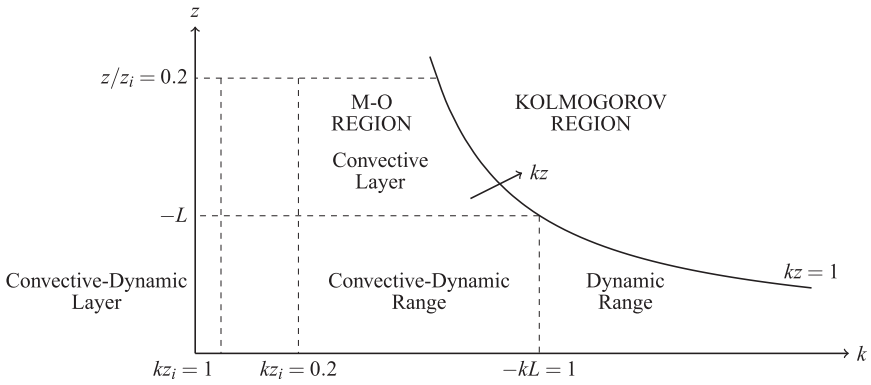

FIG. 1. Schematic of the scaling regions in the convective atmospheric surface layer.

than z/L is the main similarity parameter, since z is no longer representative of the eddy scale.

The above considerations suggest that general surface-layer similarity must explicitly include the horizontal scales, which are contained in multipoint statistics. Thus, the generalized similarity must be formulated for multipoint statistics. We hypothesize that a multipoint statistic in the surface layer ($z \ll z_i$), having length scales much smaller than the boundary layer depth, depends only on the surface-layer parameters (u_*, β, and Q), z, and its length scales. Therefore, only multipoint statistics can achieve full similarity. Formally, for $N+1$ points $\mathbf{x}_0, \mathbf{x}_1, \ldots, \mathbf{x}_N$ with $z_k \ll z_i$, forming N separation vectors $\mathbf{r}_k = \mathbf{x}_k - \mathbf{x}_0$ with $|\mathbf{r}_k| \ll z_i$, the joint probability density function (JPDF) of the velocity difference $\mathbf{v}_k = \mathbf{u}(\mathbf{x}_k) - \mathbf{u}(\mathbf{x}_0)$ for $k = 1, \ldots, N$ can be expressed as

$$P'_N(\hat{\mathbf{v}}_1, \ldots, \hat{\mathbf{v}}_N, \mathbf{r}_1, \ldots, \mathbf{r}_N, z_0, \ldots, z_N, \beta, Q, u_*) = u_*^{-3N} P_N\left(\frac{\hat{\mathbf{v}}_1}{u_*}, \ldots, \frac{\hat{\mathbf{v}}_N}{u_*}, \frac{\mathbf{r}_1}{L}, \ldots, \frac{\mathbf{r}_N}{L}, \frac{z_0}{L}\right), \quad (2)$$

where $\hat{\mathbf{v}}_k$ is the sample-space variable for $\mathbf{v}_k$ and P_N is the nondimensional JPDF. Thus, MMO is the most general form of surface-layer similarity. It provides a framework to examine the similarity properties of all statistics in the surface layer. An important class of multipoint configuration is when $\mathbf{x}_k$ are in the same horizontal plane at z, in which case the JPDF has the form

$$P'_{hN}(\hat{\mathbf{v}}_1, \ldots, \hat{\mathbf{v}}_N, \mathbf{r}_1, \ldots, \mathbf{r}_N, z, \beta, Q, u_*) = u_*^{-3N} P_{hN}\left(\frac{\hat{\mathbf{v}}_1}{u_*}, \ldots, \frac{\hat{\mathbf{v}}_N}{u_*}, \frac{\mathbf{r}_{h1}}{L}, \ldots, \frac{\mathbf{r}_{hN}}{L}, \frac{z}{L}\right), \quad (3)$$

where $\mathbf{r}_h$ is the horizontal separation vector.

In the present study, we examine in detail the similarity properties of two-point statistics ($N = 1$). For this case, Eq. (3) reduces to

$$P'(\hat{\mathbf{v}}, \mathbf{r}_h, z, \beta, Q, u_*) = u_*^{-3} P\left(\frac{\hat{\mathbf{v}}}{u_*}, \frac{\mathbf{r}_h}{L}, \frac{z}{L}\right), \quad (4)$$

where $\mathbf{v} = \mathbf{u}(\mathbf{x} + \mathbf{r}) - \mathbf{u}(\mathbf{x})$ and $\hat{\mathbf{v}}$ is its sample-space variable. The second-order structure function of $\mathbf{u}$ then is

$$\begin{aligned} D'_{ij}(\mathbf{r}_h, z) &= \langle v_i v_j \rangle = u_*^{-3} \int P_{h1}\left(\frac{\hat{\mathbf{v}}}{u_*}, \frac{\mathbf{r}_h}{L}, \frac{z}{L}\right) \hat{v}_i \hat{v}_j \, d\hat{\mathbf{v}} \\ &= u_*^2 \int P'_{h1}\left(\frac{\hat{\mathbf{v}}}{u_*}, \frac{\mathbf{r}_h}{L}, \frac{z}{L}\right) \left(\frac{\hat{v}_i}{u_*}\right) \left(\frac{\hat{v}_j}{u_*}\right) d\frac{\hat{\mathbf{v}}}{u_*^3} \\ &= u_*^2 D_{ij}\left(\frac{\mathbf{r}_h}{L}, \frac{z}{L}\right), \end{aligned} \quad (5)$$

where D'_{ij} is the nondimensional structure function. Since the spectrum of $\mathbf{u}$ and the structure function are equivalent [i.e., contain the same information (Monin and Yaglom 1975)], the former has the form

$$\psi'_{ij}(\mathbf{k}_h, z) = u_*^2 L \psi_{ij}\left(\mathbf{k}_h L, \frac{z}{L}\right), \quad (6)$$

where ψ'_{ij} and ψ_{ij} are the dimensional and nondimensional spectra, respectively. The two-dimensional spectra (ψ'_{ij} and ψ_{ij} integrated over concentric rings) have the form

$$\phi'_{ij}(k, z) = u_*^2 L \phi_{ij}\left(kL, \frac{z}{L}\right), \quad (7)$$

where k is the magnitude of $\mathbf{k}_h$. Therefore, in MMO, the stability condition is determined by both the horizontal and vertical stability parameters. For a spectrum (two-point statistic), they are kL and z/L.

To illustrate the effects of the stability condition on the different scales of the convective surface layer ($L < 0$), we show in Fig. 1 the different scaling regions in k–z space. In the surface layer (defined as, say, $z/z_i < 0.2$), the curve $kz = 1$ separates the Kolmogorov scaling (small scale) region from the MMO scaling region.

The latter also has another bound on the large-scale side ($kz_i = 0.2$). While the scaling exponents of (small scale) statistics in the Kolmogorov region do not depend on L, their magnitudes generally do. The MMO scaling region can be divided into two layers: the convective layer ($-z/L \gg 1$) and the convective–dynamic layer ($-z/L \ll 1$). The former contains one horizontal scaling range ($-kL \ll 1$); hence, the turbulence fluctuations are essentially unaffected by shear since the scales of the eddies ($1/k$) are larger than L and so is the height from the surface. The latter contains two scaling ranges: the convective–dynamic range ($-kL \ll 1$) and the dynamic range ($-kL \gg 1$). In the dynamic range ($-kL \gg 1$ and $-z/L \ll 1$), the eddies are unaffected by buoyancy since their scales are much smaller than $-L$. In the convective–dynamic range ($-kL \ll 1$ and $-z/L \ll 1$), although $-z/L \ll 1$, the eddies contributing to the fluctuations have scales larger than $-L$ and, therefore, are affected by buoyancy.

Within the framework of MMO, similarity properties for one-point statistics can be derived from multipoint statistics by eliminating the dependence on the horizontal scale (parameter reduction) (e.g., integration of spectra over wavenumber or taking the large separation limit for structure functions). In general, a one-point statistic will follow the (original) M–O similarity only when its dominant contribution comes from scales covered by the M–O similarity. The relationship between MMO and the M–O similarity will be addressed in section 5.

In the free-convective boundary layer, there exists a convection-induced stress layer near the surface, which depends on both the mixed-layer scales and the roughness height (Businger 1973; Sykes et al. 1993; Grachev et al. 1997). The turbulence statistics in this layer do not have MMO because the relevant parameters do not enter MMO.

In the following, we use MMO to predict the velocity and temperature spectra in the convective atmospheric surface layer and make preliminary comparisons with LES data. The predicted horizontal velocity spectrum for $-z/L \gg 1$ is identical to that of Kader (1988), Kader and Yaglom (1991), and Yaglom (1994). The present work focuses instead on the spectra of the horizontal and vertical velocities and temperature in the convective–dynamic layer ($-z/L \ll 1$), including the convective–dynamic range and the dynamic range.

3. Spectral predictions

In this section, we make predictions of the velocity and temperature spectra for wavenumbers $kz \ll 1$ and heights $-z/L \ll 1$. The issue of predicting shear-stress and temperature-flux cospectra will be addressed in a future work. In general, a spectrum as a function of the horizontal wavenumber vector is needed to fully represent the spectral information [see Gibbs and Fedorovich (2014) for an example of such spectra]. Nevertheless, its scaling property is generally preserved when the spectrum is integrated over a concentric ring; that is, the two-dimensional spectrum (as a function of the wavenumber magnitude) has a scaling exponent equivalent to that of the spectrum, because the direction of its maximum generally dominates the two-dimensional spectrum. Therefore, following Lumley (1967), who predicted the cospectra integrated over a spherical shell, we predict the two-dimensional spectra (i.e., the ring-integrated spectra). For $kz \ll 1$, z is much smaller than the sizes of the eddies that contribute most to the spectra. The associated horizontal fluctuations do not vary significantly with z since, for $kz \to 0$ (but $z \gg z_0$, the roughness height), their variances appear to approach finite values (Kaimal et al. 1972; Townsend 1976) and are therefore largely independent of $-z/L$. Thus, the horizontal velocity spectra have the form

$$\phi_h(k,z) = (-\kappa\beta QL)^{2/3}(-L)\phi_{uL}(-kL), \tag{8}$$

where $(-\kappa\beta QL)^{1/3}$ is the velocity scale for length scale L and $\phi_{uL}(-kL)$ is a nondimensional universal function. The region $1/z_i \ll k \ll 1/z$ can be divided into two scaling ranges. For the convective–dynamic scaling range ($1/z_i \ll k \ll -1/L$), the eddies are dominated by buoyancy effects and the spectrum should not (to the leading-order approximation) depend on u_*. Thus, we have

$$\begin{aligned}\phi_h(k) &= u_*^2\frac{u_*^3}{\kappa\beta Q}\phi_{uL}\left(k\frac{u_*^3}{\kappa\beta Q}\right)\\ &= A_h(\kappa\beta Q)^{2/3}k^{-5/3}\\ &= A_h(-\kappa\beta QL)^{2/3}(-L)(-kL)^{-5/3},\end{aligned} \tag{9}$$

where A_h is a spectral coefficient. It is important to appreciate that although the $k^{-5/3}$ dependence in Eq. (9) is formally the same as that for the convective surface layer predicted by Yaglom (1994), in the present study it is predicted using MMO for $z \ll -L$, which was previously considered to be unaffected by buoyancy. Thus, the scaling exponents are obtained with qualitatively different physics. The effects of shear (z/L) are expected to be of higher order and will be investigated in a future study.

It is interesting to note that this result can also be obtained by asymptotically matching the spectrum in Eq. (8) with the z_i-scaled spectrum,

$$\begin{aligned}\phi_h(k) &= w_*^2 z_i \phi_{uz_i}(kz_i) = (\kappa\beta Qz_i)^{2/3} z_i \phi_{uz_i}(kz_i)\\ &= (-\kappa\beta QL)^{2/3}(-L)\left(-\frac{z_i}{L}\right)^{5/3}\phi_{uz_i}(kz_i).\end{aligned} \tag{10}$$

In the overlapping region ($kz_i \to \infty$, $-kL \to 0$), the spectra given in Eqs. (8) and (10) must have the same form, leading to

$$\phi_{uz_i}(kz_i) \sim (kz_i)^{-5/3}. \tag{11}$$

For the dynamic scaling range ($-1/L \ll k \ll 1/z$), the eddies are dominated by shear and the spectrum does not depend on Q, leading to

$$\phi_h(k) = B_h u_*^2 k^{-1} = B_h u_*^2 (-L)(-kL)^{-1}, \tag{12}$$

where B_h is a spectral coefficient. To perform asymptotic matching between that given by Eq. (8) and the z-scaled spectrum,

$$\phi_h(k) = u_*^2 z \phi_{uz}(kz), \tag{13}$$

we rewrite the spectrum in Eq. (8) as

$$\phi_h(k) = u_*^2(-L)\phi_{uL}(-kL) = u_*^2 z\left(-\frac{L}{z}\right)\phi_{uL}\left(-kz\frac{L}{z}\right). \tag{14}$$

Thus, $\phi_{uL}(-kL)$ has the form $(-kL)^{-1}$ in the overlapping region. The k^{-1} dependence is the same as that in a neutral boundary layer (e.g., Laufer 1954; Pond et al. 1966; Perry and Abell 1975).

The (large scale) vertical velocity spectrum in the M–O scaling region (Fig. 1), $\phi_w(k)$, has not been predicted previously. Using continuity for the scale $1/k$, we have

$$\frac{\phi_w(k)}{z^2} \sim \frac{\phi_h(k)}{(1/k)^2}; \tag{15}$$

that is, $\phi_w(k) \sim (kz)^2 \phi_h(k)$, hence

$$\phi_w(k) = (-\kappa\beta QL)^{2/3}(-L)(kz)^2\phi_{uL}(-kL). \tag{16}$$

Therefore, for the convective–dynamic scaling range ($1/z_i \ll k \ll -1/L$), the spectrum has the form

$$\begin{aligned}\phi_w(k) &= A_w(\kappa\beta Q)^{2/3}(kz)^2 k^{-5/3}\\ &= A_w(\kappa\beta Q)^{2/3} z^2 k^{1/3}\\ &= A_w(-\kappa\beta QL)^{2/3}(-L)\left(-\frac{z}{L}\right)^2(-kL)^{1/3},\end{aligned} \tag{17}$$

where A_w is a spectral coefficient. This spectral form and that given in Eq. (9) are also applicable to the convective layer. For the dynamic range ($-1/L \ll k \ll 1/z$),

$$\phi_w(k) = B_w u_*^2 (kz)^2 k^{-1} = B_w u_*^2 z^2 k, \tag{18}$$

where B_w is a spectral coefficient.

The temperature spectrum depends on Q, β, u_*, and k, and has the general form

$$\phi_\theta(k) = \frac{Q^2}{(-\kappa\beta QL)^{2/3}}(-L)\phi_{\theta L}(-kL). \tag{19}$$

In the convective–dynamic scaling range, $\phi_\theta(k)$ does not depend on u_*, leading to

$$\phi_\theta(k) = A_\theta(\kappa\beta)^{-2/3} Q^{4/3} k^{-1/3}, \tag{20}$$

where A_θ is a spectral coefficient. This spectral form is the same as that given by Yaglom (1994); however, for $-z/L \ll 1$, it is valid for $1/z_i \ll k \ll -1/L$. In the dynamic scaling range, the spectrum does not depend on buoyancy; therefore, β vanishes. Thus, we have

$$\phi_\theta(k) = B_\theta Q^2 u_*^{-2} k^{-1} = B_\theta T_*^2 (-L)(-kL)^{-1}, \tag{21}$$

where B_θ is a spectral coefficient and $T_* = -Q/u_*$. The spectral forms predicted above are summarized in Fig. 2. We note that Kaimal (1978) observed a "transition" between the $-5/3$ scaling regions for the large-scale and the inertial ranges but did not identify it as a scaling range.

4. Comparisons of predictions with LES

In this section we compare the spectral predictions of the previous section with LES of the atmospheric boundary layer. We note that wavenumber spectra are commonly presented in (streamwise) one-dimensional form through the use of time series data and Taylor's hypothesis (e.g., Kaimal et al. 1972). Although there is general agreement on their scaling exponents with three-dimensional spectra at higher wavenumbers, one-dimensional spectra do not necessarily reflect scaling behavior at very low wavenumbers (below the integral-scale wavenumbers) because of aliasing effects (e.g., Tennekes and Lumley 1972). More specifically, Fourier modes for higher wavenumbers that are not aligned to the streamwise (or mean wind) direction appear as lower wavenumber ones in the one-dimensional spectra. Thus, the one-dimensional spectra at wavenumber k_1 contain contributions from components (in other directions) larger than k_1. In the MMO scaling range the aliasing effects most significantly affect the vertical velocity spectrum, which peaks at the highest wavenumbers of the scaling range ($1/z$). Thus, two-dimensional spectra are needed to test our prediction. We use LES, which allows for two-dimensional spectra to be obtained by integrating along concentric rings of constant horizontal wavenumber $k = (k_1^2 + k_2^2)^{1/2}$. Unlike their one-dimensional

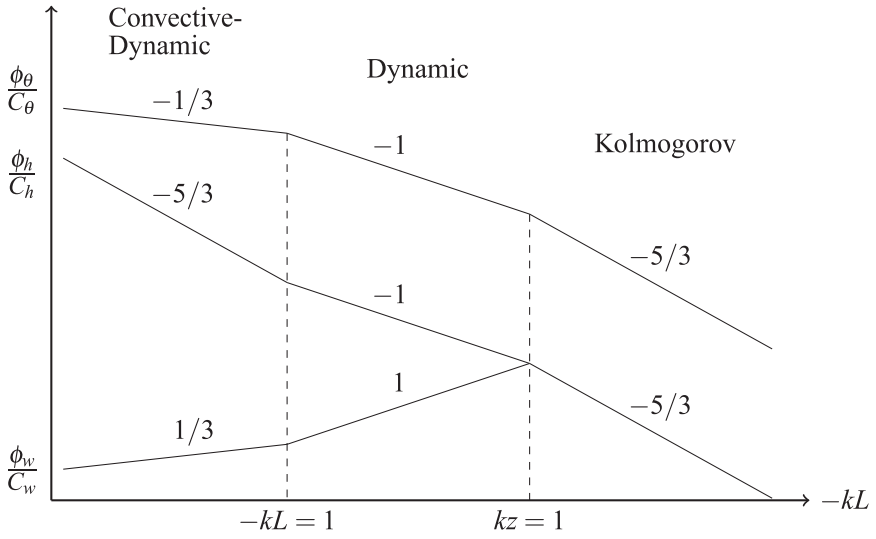

FIG. 2. Schematic of the predicted scaling of the temperature spectrum, normalized by $C_\theta = (\kappa\beta)^{-2/3} Q^{4/3} (-L)^{1/3}$, and the horizontal and vertical velocity spectra, normalized by $C_h = C_w = (\kappa\beta Q)^{2/3} (-L)^{5/3}$.

counterpart, the two-dimensional spectra vanish at zero wavenumber and properly reflect the absence of turbulent kinetic energy and scalar variance there (e.g., Peltier et al. 1996; Kelly and Wyngaard 2006). In addition, LES also allows us to test our predictions in a range of atmospheric conditions, with well-defined parameters (e.g., geostrophic winds and surface heating) that are often difficult to realize in field measurements.

The LES formulation used is presented in detail in Moeng (1984), has been well documented in the literature (Moeng and Wyngaard 1988; Sullivan et al. 1994, 1996), and includes later refinements by Otte and Wyngaard (2001). The LES code solves the spatially filtered momentum equation for Boussinesq flow and a transport equation for a filtered conserved scalar, supplemented with a transport equation for the subgrid-scale turbulent kinetic energy. A pressure Poisson equation, obtained by applying a numerical divergence operator to the momentum equation, enforces incompressibility. The numerical scheme is pseudospectral in the horizontal directions and finite difference in the vertical, the latter implemented on a staggered mesh to maintain tight velocity–pressure coupling. The nonlinear advection terms are implemented in rotational form, and aliasing errors are eliminated using an explicit sharp Fourier cutoff of the upper 1/3 wavenumbers (Canuto et al. 1988). Time stepping is performed using a third-order Runge–Kutta scheme (Spalart et al. 1991; Sullivan et al. 1996). Consistent with the pseudospectral method, periodic boundary conditions are used on the domain sidewalls. At the lower boundary, wall functions based on the Monin–Obukhov similarity are used to estimate the surface stress and flux (Businger et al. 1971). At the upper boundary, a radiative boundary condition allows for gravity waves to pass through without reflection (Klemp and Durran 1983). Neumann boundary conditions, derived from the vertical momentum equation, supplement the pressure Poisson equation.

We simulate four cases of atmospheric boundary layer flow: 1) a (nearly) neutrally stratified ABL driven by a constant large-scale pressure gradient corresponding to geostrophic wind components $(U_g, V_g) = (10, 0)\,\mathrm{m\,s^{-1}}$ (because of the stably stratified inversion at the top, the boundary layer is slightly stable even with zero surface heat flux), 2) a weakly unstable and 3) moderately unstable ABL driven by a combination of geostrophic winds and surface heating, and 4) a nearly free-convective ABL driven by a constant surface heat flux ($Q = 0.24\,\mathrm{K\,m\,s^{-1}}$) and weak geostrophic winds. The parameters for the four cases are summarized in Table 1. For all cases, the subgrid-scale (SGS) fluxes are parameterized using the Smagorinsky model (Smagorinsky 1963; Lilly 1967; Moeng 1984); for the weakly and moderately convective cases, we also employ the Kosović model (Kosović 1997), which adds a nonlinear term to the eddy-viscosity formulation to account for backscatter effects, in order to compare the effects of the SGS parameterization on the spectral forms. All simulations are implemented on a mesh of 1024^3 grid points, with a domain size of $5120^2\,\mathrm{m}^2$ in the horizontal and 2048 m in the vertical. We prescribe a surface roughness of $z_0 = 0.1\,\mathrm{m}$, Coriolis parameter $f = 1 \times 10^{-4}\,\mathrm{m\,s^{-1}}$, and an initial capping inversion at $z_i = 1024\,\mathrm{m}$. The simulations are carried forward for 25τ,

TABLE 1. Large-eddy simulation parameters.

Stability	U_g (m s^{-1})	Q (K m s^{-1})	SGS model	$-L$ (m)	z_i (m)	u_* (m s^{-1})	w_* (m s^{-1})
Neutral	10	0	Smagorinsky	∞	981	0.45	0
Weakly convective	15	0.08	Kosović	331	1015	0.70	1.38
			Smagorinsky	262	1017	0.65	1.38
Moderately convective	10	0.12	Kosović	104	1031	0.55	1.59
			Smagorinsky	84	1032	0.51	1.59
Strongly convective	1	0.24	Smagorinsky	4	1076	0.24	2.02

where $\tau = z_i/w_*$ (or u_* for the neutral case) defines one large-eddy turnover time and $w_* = (\beta Q z_i)^{1/3}$ is calculated using the initial z_i and the prescribed temperature flux. Statistics are averaged from 10τ to 25τ.

While LES has been shown to be satisfactory in predicting turbulence statistics in the mixed layer, near the surface, especially at the first few grid points, the influence of the SGS model and the boundary conditions can be significant. We take several steps to minimize such influences: First, we employ two SGS models with the same boundary conditions so that the sensitivity of the spectra to the SGS model can be assessed. Second, we evaluate the spectra obtained at several heights [8 (not shown), 16, 20, and 30 m] to assess their sensitivity to the SGS model and the boundary conditions, since they play a greater role near the surface. We found that the forms of the spectra below $z = 16$ m (the eighth grid point) begin to depart from those at greater heights, while the latter agree among themselves. Third, we also obtain LES fields at a different resolution (512^3), which helps us to further assess sensitivity to the SGS model and the boundary conditions. The results show that the variability of the results is small compared to the variations of the spectra and does not affect the identification of the scaling ranges. Therefore, the LES spectra obtained in the present study are sufficiently accurate for testing the spectral forms predicted using MMO. We note that comparing the nondimensional spectra at different heights also provides a test of the MMO scaling (different z but the same z/L).

We first compare the spectra obtained from LES to previous predictions of the horizontal velocity spectrum for the neutral (e.g., Perry and Abell 1975) and strongly convective surface layers (Yaglom 1994). Our predictions of the vertical velocity and temperature spectra [Eqs. (17), (18), (20), and (21)] are also compared to those obtained from LES. The horizontal and vertical velocity spectra in the neutral surface layer obtained using the Smagorinsky model at $z = 16$, 20, and 30 m are shown in Fig. 3. The dynamic scaling range ($1/z_i \ll k \ll 1/z$) extends to very low wavenumbers and covers nearly two decades. The spectral forms in this range show the predicted k^{-1} scaling for the horizontal velocity spectrum [Eq. (12)] and k^1 for the vertical velocity spectrum [Eq. (18)], followed by $k^{-5/3}$ in the Kolmogorov region. We note that the one-dimensional spectrum of the vertical velocity (not shown) is nondecreasing as k approaches zero and does not contain the k^1 range due to aliasing. It is common practice to premultiply the spectrum by k to indicate that the spectral contents decrease with k (e.g., Kaimal et al. 1972; Wyngaard 2010). However, the resulting premultiplied spectra do not have the correct k dependence.

Figure 4 shows the velocity and temperature spectra in the nearly freely convective surface layer obtained using the Smagorinsky model. For this case, the wavenumbers corresponding to the energy-containing eddies lie entirely within the convective scaling range ($1/z_i \ll k \ll -1/L$). The horizontal velocity spectrum largely follows the predicted $k^{-5/3}$ power law [Eq. (9)]. There is a transition region (near $kz = 1$) between the convective–dynamic and inertial subranges (which have the same $k^{-5/3}$ dependence but different functional magnitudes). The vertical velocity spectrum exhibits the predicted $k^{1/3}$ form [Eq. (17)] for $k < 1/z$; for $k > 1/z$, it transitions to the $k^{-5/3}$ inertial-range form. Similarly, the temperature spectrum follows the predicted $k^{-1/3}$ form [Eq. (20)] for $k < 1/z$, followed by $k^{-5/3}$ in the inertial subrange.

We test our predictions of the spectra in the convective–dynamic layer using LES of the weakly convective and moderately convective ABL. Figures 5 and 6 show the velocity and temperature spectra in the surface layer of the weakly convective ABL ($z_i/L \approx -3.5$) obtained using the Smagorinsky and Kosović models, respectively. The spectra appear to collapse in the wavenumber range $4 \times 10^{-1} \leq -kL \leq 5$, only diverging at higher wavenumbers (approaching $kz = 1$), supporting the MMO scaling. Because of the weak surface heating, there is only a small band of low wavenumbers in the convective–dynamic scaling range ($-kL < 3$), where the vertical velocity and temperature spectra appear to follow the

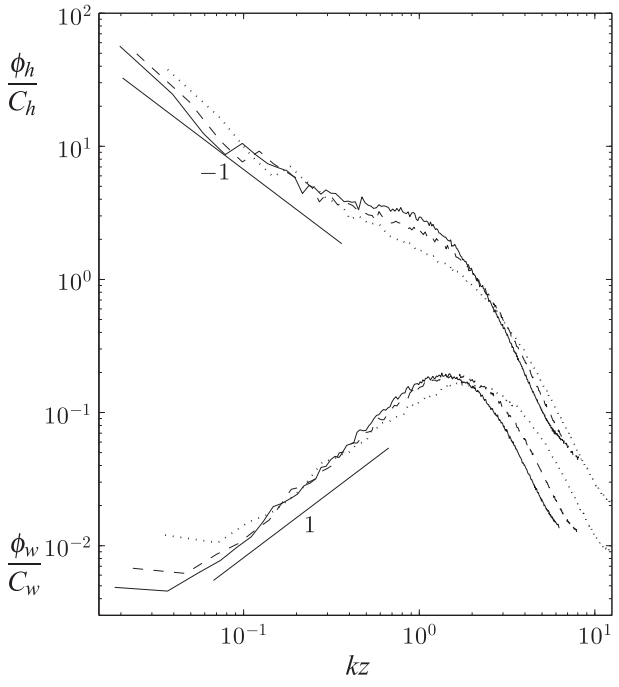

FIG. 3. Horizontal and vertical velocity spectra for the neutral ABL, normalized by $C_h = C_w = u_*^2 z$. The lines represent 16 (solid), 20 (dashed), and 30 m (dotted). For clarity, ϕ_w has been multiplied by 5×10^{-1}.

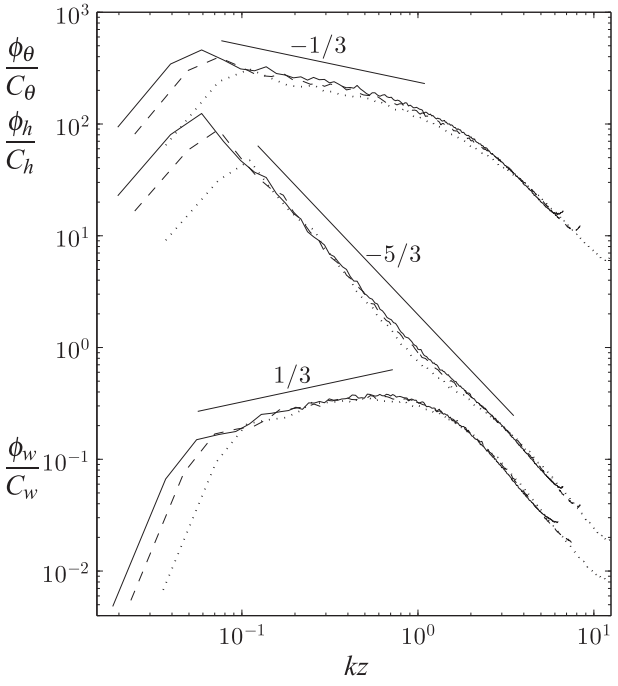

FIG. 4. Temperature and velocity spectra for the nearly free-convective ABL, normalized by $C_\theta = (\kappa\beta)^{-2/3} Q^{4/3} z^{1/3}$ and $C_h = C_w = (\kappa\beta Q)^{2/3} z^{5/3}$. The lines represent 16 (solid), 20 (dashed), and 30 m (dotted). For clarity, ϕ_θ has been multiplied by 5×10^2 and ϕ_w has been multiplied by 2.5×10^{-1}.

predicted $k^{1/3}$ and $k^{-1/3}$ forms [Eqs. (17) and (20), respectively]. The horizontal velocity spectrum appears to transition toward the predicted $k^{-5/3}$ form [Eq. (9)]. In the dynamic scaling range, the vertical velocity spectrum is close to the predicted k^1 scaling over one decade ($-L/z \approx 15$). The horizontal velocity and temperature spectra appear to approach the predicted k^{-1} form at higher wavenumbers ($-kL < 10$) within the dynamic subrange. The scaling ranges appear to be better defined for the Kosović model than the Smagorinsky model. We note that similar scaling of the temperature and horizontal velocity spectra in this range reflects the passive role of temperature in the shear-dominated dynamic layer.

For the moderately convective ABL ($-z_i/L \approx 11$), the convective–dynamic scaling range is more evident. The horizontal and vertical velocity spectra, shown in Figs. 7 and 8 (obtained using the Smagorinsky and Kosović models, respectively), largely follow the predicted $k^{-5/3}$ and $k^{1/3}$ forms in the convective–dynamic subrange. The temperature spectrum follows the predicted $k^{-1/3}$ form over one decade. Because of the smaller scale separation between z ($\leq$30 m) and $-L$ ($\sim$100 m), the dynamic subrange covers a smaller band of wavenumbers near $-kL = 2$, where the horizontal velocity and temperature spectra are close to the predicted k^{-1} form. The transition between the convective–dynamic and dynamic scaling ranges is less obvious for the vertical velocity spectrum, although its slope does appear to increase somewhat toward the predicted k^1 form at higher wavenumbers within the dynamic scaling range, before falling off as $k^{-5/3}$ in the inertial subrange.

The predicted horizontal velocity spectrum [Eqs. (9) and (12)] in the convective–dynamic layer and that obtained from the LES are also consistent with the spectrum observed by Kaimal (1978) and the proposed empirical form (obtained using field measurement data). Although a transitional range between the inertial range and the large scales was observed and noted in Kaimal (1978), it was not recognized as a scaling range (the dynamic range). In addition, the parameter kL did not play a role in the scaling of their spectrum.

The spectra obtained from LES are in general agreement with the MMO predictions, both in terms of the scaling exponents and the consistency of the spectral coefficients. We note that the spectral predictions in the present study, including the predictions of the scaling exponents and spectral coefficients, are made for asymptotically large-scale separations ($z_i \gg -L \gg z$). Thus, the limited scaling ranges and the approximate scaling exponents observed are a result of the limited scale separations ($-z_i/L$ and $-L/z$). As noted above, the shapes of the spectra near $k = 1/z$ obtained at

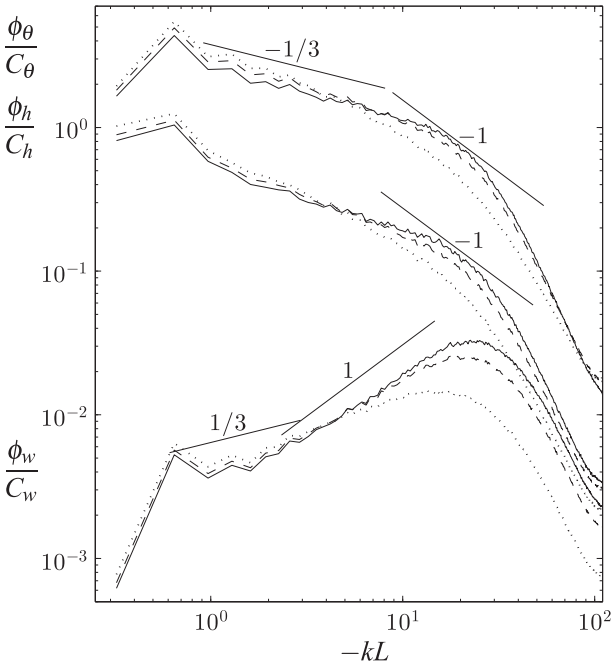

FIG. 5. Temperature and velocity spectra for the weakly convective ABL using the Smagorinsky model, normalized by $C_\theta = (\kappa\beta)^{-2/3}Q^{4/3}(-L)^{1/3}$, $C_h = (-\kappa\beta QL)^{2/3}(L)$, and $C_w = (-\kappa\beta QL)^{2/3}z^2(-L)^{-1}$. The lines represent 16 (solid), 20 (dashed), and 30 m (dotted). For clarity, ϕ_θ has been multiplied by 7.5 and ϕ_w has been multiplied by 5×10^{-3}.

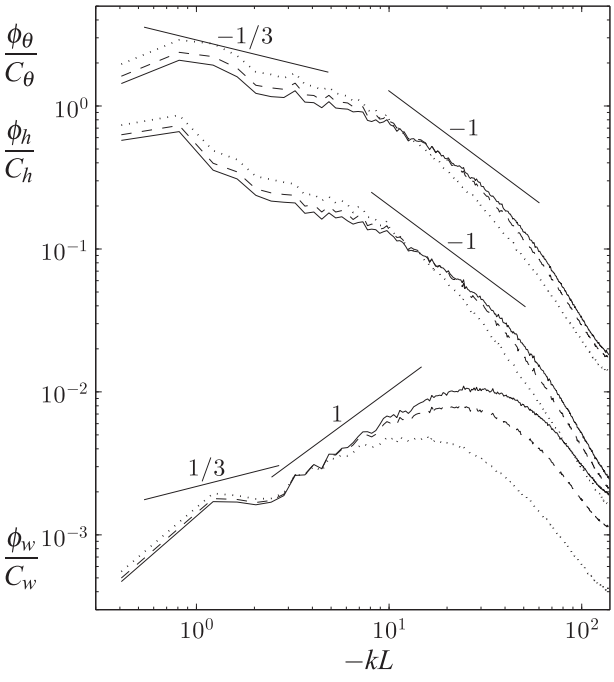

FIG. 6. Temperature and velocity spectra for the weakly convective ABL using the Kosović model, normalized as in Fig. 5. The lines represent 16 (solid), 20 (dashed), and 30 m (dotted). For clarity, ϕ_θ has been multiplied by 7.5 and ϕ_w has been multiplied by 1.5×10^{-3}.

$z = 16$ m (the eighth grid point) begin to show departures from those at higher z, presumably because of the limited resolution. The results for 512^3 LES (not shown) also have the same trend. Therefore, the eighth grid point appears to be the lowest height to obtain relatively accurate spectra for testing the MMO predictions. Further comparisons with LES at higher resolutions, which allow for larger-scale separations, as well as with field measurements with suitable stability conditions, are needed.

5. Relationship between MMO and the original M–O similarity

MMO is formulated in terms of the JPDF of multipoint velocity and scalar differences, because only such multipoint statistics can achieve full similarity. The similarity properties (or a lack thereof) for one-point statistics (in the sense of the original M–O similarity) can be derived from multipoint statistics by eliminating the dependence on the horizontal scale (separation or wavenumber). For example, a velocity variance can be obtained by integrating the spectrum or by taking the large separation limit of the related second-order structure function. Therefore, the M–O similarity is a special case of MMO. In general, a one-point statistic follows the M–O similarity if its dominant contributions come from length scales that scale with z. For example, the horizontal and vertical velocity variances in the convective–dynamic layer can be obtained by integrating ϕ_h and ϕ_w over k. In the convective boundary layer, the form of σ_α^2 for $-z/L < 1$ therefore contains contributions from the convective–dynamic, dynamic, and Kolmogorov (inertial) subranges: $1/z_i \ll k \ll -1/L$, $-1/L \ll k \ll 1/z$, and $1/z \ll k \ll 1/\eta$, respectively. The contributions from the convective–dynamic subrange depend on z_i/L, while those from the dynamic and Kolmogorov subranges depend on z/L [the Kolmogorov subrange depends on the dissipation rate $\phi_\varepsilon(z/L)$; e.g., the functional forms given by Kaimal et al. (1972) and Caughey and Wyngaard (1979)]. The velocity variances therefore depend on both z/L and z_i/L. However, because the dominant contributions to the horizontal velocity variances have length scales comparable to z_i (corresponding to wavenumbers in the convective–dynamic subrange of scale $k \sim 1/z_i \ll -1/L$), their dependence on z/L vanishes (or becomes asymptotically weak compared to that on z_i/L). Therefore, the horizontal velocity variances are not M–O similar. On the other hand, the dominant contributions to the vertical velocity variance come from much smaller eddies with length scales comparable to z ($\ll -L$) (corresponding to wavenumbers in the dynamic subrange,

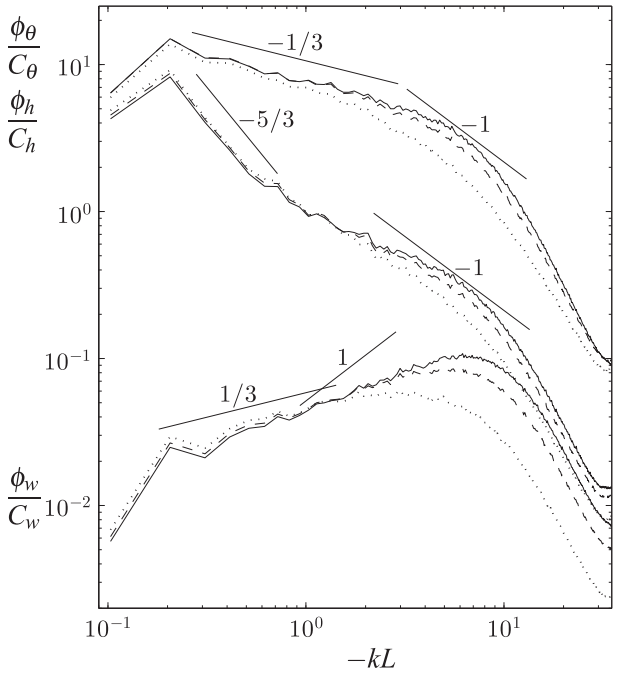

FIG. 7. Temperature and velocity spectra for the moderately convective ABL using the Smagorinsky model, normalized as in Fig. 5. The lines represent 16 (solid), 20 (dashed), and 30 m (dotted). For clarity, ϕ_θ has been multiplied by 15 and ϕ_w has been multiplied by 4×10^{-2}.

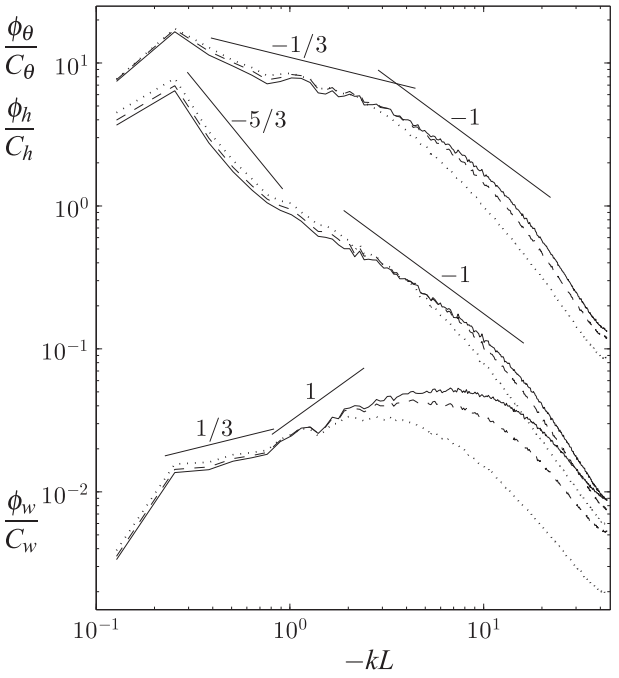

FIG. 8. Temperature and velocity spectra for the moderately convective ABL using the Kosović model, normalized as in Fig. 5. The lines represent 16 (solid), 20 (dashed), and 30 m (dotted). For clarity, ϕ_θ has been multiplied by 20 and ϕ_w has been multiplied by 2×10^{-2}.

bounded below by $k \sim 1/L$) and, therefore, are asymptotically independent of z_i/L. Thus, the vertical velocity variance follows M–O similarity.

The M–O similarity has also been widely applied to mean gradients in the surface layer (e.g., Businger et al. 1971). While the similarity properties of one-point statistics of turbulence fluctuations can be directly derived from MMO through parameter reduction, those of the mean gradients require additional considerations as MMO does not include mean quantities. To relate the mean gradients to the fluctuation statistics, equations containing the mean gradients are needed. For example, the transport equation for the horizontal velocity variance contains the mean shear and can be used to deduce the similarity properties of the latter. In such an analysis the similarity properties of all the fluctuation statistics must be considered. In general, a mean gradient is M–O similar only if all the fluctuation statistics in its transport equation are. This issue will be investigated in future research.

6. Conclusions

A generalized M–O similarity, termed multipoint Monin–Obukhov similarity, is proposed and includes the Monin–Obukhov length as a scale in both the horizontal and vertical directions, as opposed to only the vertical direction in the (original) M–O similarity. MMO is formulated for the JPDF of the multipoint velocity-scalar differences, stating that the nondimensional JPDF is a function of the nondimensional separations $\mathbf{r}_{h1}/L$, $\mathbf{r}_{h2}/L$, ..., $\mathbf{r}_{hN}/L$ and the nondimensional height z_0/L.

We use MMO to predict two-dimensional velocity and temperature spectra (as a function of the horizontal wavenumber magnitude) in the convective surface layer, which are two-point statistics having two independent variables: kL and z/L. MMO predicts three scaling ranges: the convective range for $1/z_i \ll k \ll -1/L$ and $-z/L \gg 1$, the convective–dynamic range for $1/z_i \ll k \ll -1/L$ and $-z/L \ll 1$, and the dynamic range for $-1/L \ll k \ll 1/z$ and $-z/L \ll 1$. The spectral predictions are in general agreement with high-resolution LES data, providing support for MMO. We note that the (original) M–O similarity does not lead to correct scaling of the spectra for $-z/L \ll 1$. In addition, to our best knowledge, ours is the first prediction of the vertical velocity spectrum for the M–O scaling region.

MMO predicts a two-layer structure for the convective surface layer. Betchov and Yaglom (1971) considered $-z/L \approx 1$ as a separate layer. MMO shows that it is not a separate layer (i.e., one with different scaling exponents). MMO predictions of the spectra in the convective layer and in the convective–dynamic range in the

convective–dynamic layer have the same form, which is supported by the available data. The prediction is made for asymptotically large-scale separations ($z_i \gg -L \gg z$). For finite values of the separation, it is likely that there will be some dependence of the convective–dynamic range on z/L; therefore, the results in the present work are the leading-order approximations. Corrections accounting for the departure for small z/L are of higher order and will require analyses of the dynamic equations of the spectra.

While the similarity properties for the velocity and temperature spectra are considered in the present work, other statistics such as the horizontal structure functions can also be analyzed. Any similarity properties (or a lack thereof) for one-point statistics can be derived from two-point statistics. Such analyses will be important for understanding the budget equations for one-point statistics. To this end, MMO provides a new framework for understanding the atmospheric surface layer, especially the convective surface layer.

Acknowledgments. We thank Dr. Martin J. Otte at the U.S. Environmental Protection Agency for providing the LES code and help in its implementation. This work was supported by the National Science Foundation through Grant ATM-1335995.

REFERENCES

Betchov, R., and A. M. Yaglom, 1971: Comments on the theory of similarity as applied to turbulence in an unstable stratified fluid. *Izv. Akad. Nauk SSSR, Fiz. Atmos. Okeana*, **7**, 829–832.

Bradshaw, P., 1978: Comments on "Horizontal velocity spectra in an unstable surface layer." *J. Atmos. Sci.*, **35**, 1768–1769, doi:10.1175/1520-0469(1978)035<1768:COVSIA>2.0.CO;2.

Businger, J. A., 1973: A note on free convection. *Bound.-Layer Meteor.*, **4**, 323–326, doi:10.1007/BF02265241.

——, J. C. Wyngaard, Y. Izumi, and E. F. Bradley, 1971: Flux-profile relationships in the atmospheric surface layer. *J. Atmos. Sci.*, **28**, 181–189, doi:10.1175/1520-0469(1971)028<0181:FPRITA>2.0.CO;2.

Canuto, C., M. Y. Hussaini, A. Quarteroni, and T. A. Zang, 1988: *Spectral Methods in Fluid Dynamics*. Springer-Verlag, 567 pp.

Caughey, S. J., and J. C. Wyngaard, 1979: The turbulence kinetic energy budget in convective conditions. *Quart. J. Roy. Meteor. Soc.*, **105**, 231–239, doi:10.1002/qj.49710544315.

Gibbs, J. A., and E. Fedorovich, 2014: Comparison of convective boundary layer velocity spectra retrieved from large-eddy-simulation and Weather Research and Forecasting Model data. *J. Appl. Meteor. Climatol.*, **53**, 377–394, doi:10.1175/JAMC-D-13-033.1.

Grachev, A. A., C. W. Fairall, and S. S. Zilitinkevich, 1997: Surface-layer scaling for the convection induced stress regime. *Bound.-Layer Meteor.*, **83**, 423–439, doi:10.1023/A:1000281625985.

Kader, B. A., 1988: Three-layer structure of an unstably stratified atmospheric surface layer. *Izv. Akad. Nauk SSSR, Fiz. Atmos. Okeana*, **24**, 907–918.

——, and A. M. Yaglom, 1991: Spectra and correlation functions of surface layer atmospheric turbulence in unstable thermal stratification. *Turbulence and Coherent Structures*, M. Lesieur and O. Métais, Eds., Kluwer, 387–412.

Kaimal, J. C., 1978: Horizontal velocity spectra in an unstable surface layer. *J. Atmos. Sci.*, **35**, 18–24, doi:10.1175/1520-0469(1978)035<0018:HVSIAU>2.0.CO;2.

——, J. C. Wyngaard, Y. Izumi, and O. R. Coté, 1972: Spectral characteristic of surface-layer turbulence. *Quart. J. Roy. Meteor. Soc.*, **98**, 563–589, doi:10.1002/qj.49709841707.

Kelly, M., and J. C. Wyngaard, 2006: Two-dimensional spectra in the atmospheric boundary layer. *J. Atmos. Sci.*, **63**, 3066–3070, doi:10.1175/JAS3769.1.

Klemp, J. B., and D. R. Durran, 1983: An upper boundary condition permitting internal gravity wave radiation in numerical mesoscale models. *Mon. Wea. Rev.*, **111**, 430–444, doi:10.1175/1520-0493(1983)111<0430:AUBCPI>2.0.CO;2.

Kosović, B., 1997: Subgrid-scale modelling for the large-eddy simulation of high-Reynolds-number boundary layers. *J. Fluid Mech.*, **336**, 151–182, doi:10.1017/S0022112096004697.

Laufer, J., 1954: The structure of turbulence in fully developed pipe flow. NACA Tech. Rep. 1174, 417–434. [Available online at http://naca.central.cranfield.ac.uk/reports/1954/naca-report-1174.pdf.]

Lilly, D. K., 1967: The representation of small-scale turbulence in numerical simulation experiments. *Proc. Scientific Computing Symp. on Environmental Science*, Yorktown Heights, NY, IBM, 195–210.

Lumley, J. L., 1967: Similarity and the turbulent energy spectrum. *Phys. Fluids*, **10**, 855–858, doi:10.1063/1.1762200.

——, and H. A. Panofsky, 1964: *The Structure of Atmospheric Turbulence.* Interscience Monographs and Texts in Physics and Astronomy, Vol. 12, Interscience Publishers, 239 pp.

Moeng, C.-H., 1984: A large-eddy simulation model for the study of planetary boundary-layer turbulence. *J. Atmos. Sci.*, **41**, 2052–2062, doi:10.1175/1520-0469(1984)041<2052:ALESMF>2.0.CO;2.

——, and J. C. Wyngaard, 1988: Spectral analysis of large-eddy simulations of the convective boundary layer. *J. Atmos. Sci.*, **45**, 3573–3587, doi:10.1175/1520-0469(1988)045<3573:SAOLES>2.0.CO;2.

Monin, A. S., and A. M. Obukhov, 1954: Basic laws of turbulent mixing in the ground layer of the atmosphere. *Tr. Geofiz. Inst., Akad. Nauk SSSR*, **151**, 163–187.

——, and A. M. Yaglom, 1975: *Statistical Fluid Mechanics.* MIT Press, 874 pp.

Nguyen, K. X., and C. Tong, 2015: Investigation of subgrid-scale physics in the convective atmospheric surface layer using the budgets of the conditional mean subgrid-scale stress and temperature flux. *J. Fluid Mech.*, **772**, 295–329, doi:10.1017/jfm.2015.171.

——, T. W. Horst, S. P. Oncley, and C. Tong, 2013: Measurements of the budgets of the subgrid-scale stress and temperature flux in a convective atmospheric surface layer. *J. Fluid Mech.*, **729**, 388–422, doi:10.1017/jfm.2013.302.

——, M. J. Otte, E. G. Patton, P. P. Sullivan, and C. Tong, 2014: Investigation of the pressure–strain-rate correlation using high-resolution LES of the atmospheric boundary layer. *Proc. 67th Annual Meeting of the APS Division of Fluid Dynamics*, San Francisco, CA, American Physical Society, L27.00003. [Available online at http://meetings.aps.org/Meeting/DFD14/Session/L27.3.]

Otte, M. J., and J. C. Wyngaard, 2001: Stably stratified interfacial-layer turbulence from large-eddy simulation. *J. Atmos. Sci.*, **58**, 3424–3442, doi:10.1175/1520-0469(2001)058<3424:SSILTF>2.0.CO;2.

Panofsky, H. A., and J. Dutton, 1984: *Atmospheric Turbulence.* Wiley-Interscience, 397 pp.

Peltier, L. J., J. C. Wyngaard, S. Khanna, and J. Brasseur, 1996: Spectra in the unstable surface layer. *J. Atmos. Sci.*, **53**, 49–61, doi:10.1175/1520-0469(1996)053<0049:SITUSL>2.0.CO;2.

Perry, A. E., and C. J. Abell, 1975: Scaling laws for pipe-flow turbulence. *J. Fluid Mech.*, **67**, 257–271, doi:10.1017/S0022112075000298.

Pond, S., S. D. Smith, P. F. Hamblin, and R. W. Burling, 1966: Spectra of velocity and temperature fluctuations in the atmospheric boundary layer over the sea. *J. Atmos. Sci.*, **23**, 376–386, doi:10.1175/1520-0469(1966)023<0376:SOVATF>2.0.CO;2.

Smagorinsky, J., 1963: General circulation experiments with the primitive equations: I. The basic equations. *Mon. Wea. Rev.*, **91**, 99–164, doi:10.1175/1520-0493(1963)091<0099:GCEWTP>2.3.CO;2.

Spalart, P. R., R. D. Moser, and M. M. Rogers, 1991: Spectral methods for the Navier-Stokes equations with one infinite and two periodic directions. *J. Comput. Phys.*, **96**, 297–324, doi:10.1016/0021-9991(91)90238-G.

Sullivan, P. P., J. C. McWilliams, and C.-H. Moeng, 1994: A subgrid-scale model for large-eddy simulation of planetary boundary-layer flows. *Bound.-Layer Meteor.*, **71**, 247–276, doi:10.1007/BF00713741.

——, ——, and ——, 1996: A grid nesting method for large-eddy simulation of planetary boundary-layer flows. *Bound.-Layer Meteor.*, **80**, 167–202, doi:10.1007/BF00119016.

Sykes, R. I., D. S. Henn, and W. S. Lewellen, 1993: Surface-layer description under free-convection conditions. *Quart. J. Roy. Meteor. Soc.*, **119**, 409–421, doi:10.1002/qj.49711951103.

Tennekes, H., and J. L. Lumley, 1972: *A First Course in Turbulence.* MIT Press, 320 pp.

Townsend, A. A., 1961: Equilibrium layers and wall turbulence. *J. Fluid Mech.*, **11**, 97–120, doi:10.1017/S0022112061000883.

——, 1976: *The Structure of Turbulent Shear Flows.* Cambridge University Press, 429 pp.

Willis, G. E., and J. W. Deardorff, 1974: A laboratory model of the unstable planetary boundary layer. *J. Atmos. Sci.*, **31**, 1297–1307, doi:10.1175/1520-0469(1974)031<1297:ALMOTU>2.0.CO;2.

Wyngaard, J. C., 2010: *Turbulence in the Atmosphere.* Cambridge University Press, 406 pp.

——, and O. R. Coté, 1971: The budgets of turbulent kinetic energy and temperature variance in the atmospheric surface layer. *J. Atmos. Sci.*, **28**, 190–201, doi:10.1175/1520-0469(1971)028<0190:TBOTKE>2.0.CO;2.

——, ——, and Y. Izumi, 1971: Local free convection, similarity, and the budgets of shear stress and heat flux. *J. Atmos. Sci.*, **28**, 1171–1182, doi:10.1175/1520-0469(1971)028<1171:LFCSAT>2.0.CO;2.

Yaglom, A. M., 1994: Fluctuation spectra and variances in convective turbulent boundary layers: A reevaluation of old models. *Phys. Fluids*, **6**, 962–972, doi:10.1063/1.868328.

Zilitinkevich, S. S., 1971: On the turbulence and diffusion under free convection conditions. *Izv. Akad. Nauk SSSR, Fiz. Atmos. Okeana*, **7**, 1263–1269.